Received: 8 December 2017 | Revised: 6 February 2018 | Accepted: 21 February 2018

DOI: 10.1002/bio.3482

RESEARCH ARTICLE

WILEY LUMINESCENCE
The Journal of Biological and Chemical Luminescence

Synthesis and luminescence properties of novel 8-hydroxyquinoline derivatives and their Eu(III) complexes

Yongqiang Wu[1,2] | Tiantong Guo[3] | Dehua Shu[4] | Wu Zhang[1] | Fangfei Luan[1] | Ling Shi[1] | Dongcai Guo[1,2]

[1] School of Chemistry and Chemical Engineering, Hunan University, Changsha, China

[2] Hunan Provincial Key Laboratory for Cost-effective Utilization of Fossil Fuel Aimed at Reducing Carbon-dioxide Emissions, Changsha, China

[3] School of Chemistry and Molecular Sciences, Wuhan University, Wuhan, China

[4] China Geo Engineering Corporation, Beijing, China

Correspondence
Dongcai Guo, School of Chemistry and Chemical Engineering, Hunan University, Changsha 410082, China.
Email: dcguo2001@hnu.edu.cn

Funding information
China Outstanding Engineer Training Plan for Students of Chemical Engineering & Technology in Hunan University, Grant/Award Number: 2011-40; Innovative Research Team in University, Grant/Award Number: IRT1238; Changsha Science&Technology Bureau, Grant/Award Numbers: kq1701164 and kq1701029; Hunan Provincial Science&Technology Department, Grant/Award Number: 2016SK2064; Natural Science Foundation of Hunan Province, Grant/Award Number: 11JJ5005; National Natural Science Foundation of China, Grant/Award Numbers: 21341010, J1210040 and J1103312

Abstract

Six novel 8-hydroxyquinoline derivatives were synthesized using 2-methyl-8-hydroxyquinoline and para-substituted phenol as the main starting materials, and were characterized by ^{1}H nuclear magnetic resonance (NMR), mass spectrometry (MS), ultraviolet (UV) light analysis and infra-red (IR) light analysis. Their complexes with Eu(III) were also prepared and characterized by elemental analysis, molar conductivity, UV light analysis, IR light analysis, and thermogravimetric–differential thermal analysis (TG–DTA). The results showed that the ligand coordinated well with Eu(III) ions and had excellent thermal stability. The structure of the target complex was $EuY^{1-6}(NO_3)_3.2H_2O$. The luminescence properties of the target complexes were investigated, the results indicated that all target complexes had favorable luminescence properties and that the introduction of an electron-donating group could enhance the luminescence intensity of the corresponding complexes, but the addition of an electron-withdrawing group had the opposite effect. Among all the target complexes, the methoxy-substituted complex ($-OCH_3$) had the highest fluorescence intensity and the nitro-substituted complex ($-NO_2$) had the weakest fluorescence intensity. The results showed that 8-hydroxyquinoline derivatives had good energy transfer efficiency for the Eu(III) ion. All the target complexes had a relatively high fluorescence quantum yield. The fluorescence quantum yield of the complex $EuY^3(NO_3)_3.2H_2O$ was highest among all target complexes and was up to 0.628. Because of excellent luminescence properties and thermal stabilities of the Eu(III) complexes, they could be used as promising candidate luminescent materials.

KEYWORDS

8-hydroxyquinoline derivatives, Eu(III) complexes, luminescence, synthesis

1 | INTRODUCTION

As a new type of functional material, rare earth complexes have attracted increasing attention from chemical, physical, biological and material scientists due to their unique magnetic, optical and electrical properties. As 8-hydroxyquinoline possesses *N*-containing heterocyclic and aromatic rings, and has good planar structure, conjugation and a plurality of coordination sites with an electron donor, it is within the class of chelating performance, luminescence properties and coordination metal ions as excellent materials; it is widely used in the construction of novel functional metal–organic complexes.[1–4] In recent years, the application of rare earth complexes has mainly focused on fluorescence, magnetism, gas separation and adsorption, catalysis and biomedicine.[5–8] In particular, rare earth complexes with

Abbreviations: DMF, dimethyl formamide; DMSO, dimethyl sulfide; DTA, differential thermal analysis; IR, infra-red; MS, mass spectrometry; NMR, nuclear magnetic resonance; TG, thermogravimetric; TMS, tetramethylsilane; UV, ultraviolet.

good luminescence properties have been widely used in fluorescent anti-counterfeiting materials, printing inks, as fluorescent probes and in other fields.[9–11] The 8-hydroxyquinoline rare earth and transition metal complexes have excellent optical properties. Therefore, they have become the focus of design and synthesize of novel rare earth complexes with good planar structures and luminescence properties.

To obtain good luminescent materials, a series of new 8-hydroxyquinoline derivatives and their complexes with Eu(III) was designed, synthesized and characterized. The luminescence properties of the Eu(III) complexes were studied by fluorescence spectroscopy. The fluorescence quantum yields of the Eu(III) complexes were calculated by the reference method. The design and synthesis routes for the ligands Y^{1-6} are shown in Scheme 1. Using 2-methyl-8-hydroxyquinoline and para-substituted phenol as main starting materials, 2-methyl-8-hydroxyquinoline was first refluxed with acetic anhydride to obtain the intermediate. Then, 1,4-dioxane as solvent and SeO_2 as catalyst were used to make 2-formyl-8-hydroxyquinoline. Finally, the material was condensed with para-substituted phenoxy acetyl hydrazine to obtain six novel 8-hydroxyquinoline derivatives.

2 | EXPERIMENTAL

All solvents and reagents were purchased from commercial suppliers. $Eu(NO_3)_3$ (0.1 mol L^{-1}) was prepared according to protocols described in the literature.[12] ^1H nuclear magnetic resonance (NMR) spectra were recorded on a Bruker spectrophotometer (400 MHz) using DMSO-d_6/$CDCl_3$ as the solvent and tetramethylsilane (TMS) as an internal standard. Mass spectra were registered on a high resolution mass spectrometer MAT95XP. The elemental analyses were determined using a Flash EA 1112 elemental composition analyzer manufactured in the USA. The UV spectra were measured using a LabTech UV-2100 spectrophotometer, with dimethyl sulfoxide (DMSO) as the solvent and reference. Infra-red (IR) spectra (400–4000 cm^{-1}) were obtained in KBr discs using the PERKIN–ELMER Spectrum One instrument. Melting points were determined using an X-4 binocular microscope. Thermal gravimetric analyses were carried out in a static air atmosphere on a Shimadzu DTG-60 thermogravimetric analyzer at a heating rate of 10°C/min. The fluorescence spectra were measured with a Hitachi F-2700 fluorescence spectrophotometer, with a scanning speed of 1200 nm/min and a measurement voltage of 400 V. The luminescence properties of the Eu(III) complexes were measured with a 5.0 nm slit width in the solid state. The fluorescence quantum yields (Φ_{fx}) were calculated by a comparative method using the following equation:[13,14]

$$\Phi_{fx} = \frac{n_x^2}{n_{std}^2} \cdot \frac{Fx}{F_{std}} \cdot \frac{A_{std}}{A_x} \cdot \Phi_{fstd}$$

In this experiment, n_x was approximately equal to the refractive index of the solvent, the solvent used in this experiment was DMSO, so the n_x value was approximately 1.480, the n_{std} for the water refractive index had a value of about 1.337. F denoted the integrated area in the fluorescence spectrum, and A denoted the absorbance in the ultraviolet spectrum. Φ_{fstd} was the fluorescence quantum yield of the standard solution, quinine sulfate (1.0 μg ml^{-1}) in sulfuric acid solution (0.1 mol L^{-1}) was used as a standard reference, and the Φ_{fstd} was 0.55. Fluorescence spectra were measured in DMSO solution, and the slit width was 5.0 nm.

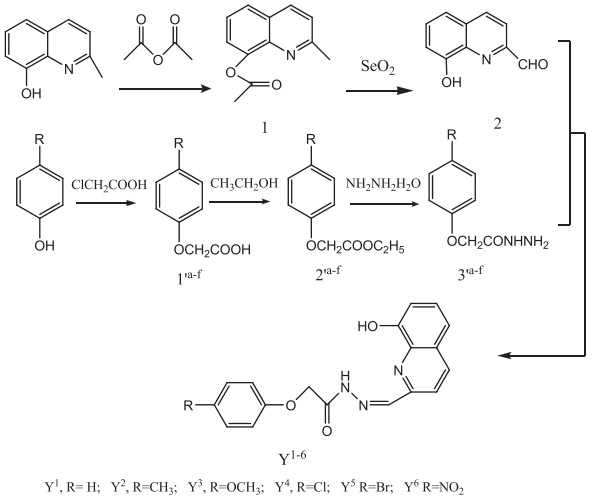

SCHEME 1 The synthesis routes for the ligands Y^{1-6}

2.1 | Synthesis of intermediate

2.1.1 | Synthesis of 2-methyl-8-acetoxy-quinoline (1)

2-Methyl-8-hydroxyquinoline (0.05 mol, 7.95 g) was added into a 100 ml three-neck flask, followed by addition of 60 ml of acetic anhydride as a solvent and reactant, the reaction mixture was heated to 138°C and refluxed for 5 h with stirring in the oil bath. The mixture was then dissolved in 100 ml dichloromethane and washed with anhydrous sodium bicarbonate solution, and dried over anhydrous magnesium sulfate, suction filtered, and evaporated to get the pale yellow oily liquid product (2-methyl-8-acetoxy-quinoline), with a 95% yield. ^1H NMR (400 MHz, $CDCl_3$) δ 8.04 (d, J = 8.4 Hz, 1H, ArH), 7.60 (dd, J = 1.5, 8.0 Hz, 1H, ArH), 7.46 (t, J = 8.0 Hz, 1H, ArH), 7.42 (d, J = 1.5 Hz, 1H, ArH), 7.25 (d, J = 8.3 Hz, 1H, ArH), 2.75 (s, 3H, CH_3). 2.51 (s, 3H, CH_3) MS (ESI) m/z (%): 201 (M + 1, 2), 158 (100).

2.1.2 | Synthesis of 2-formyl-8-hydroxyquinoline (2)

1,4-Dioxane (60 ml) and selenium dioxide (4.44 g, 0.04 mol) were added in succession in a 150 ml three-neck flask which was equipped with a reflux condenser, constant pressure dropping funnel, and a magnetic stirrer. Then 2-methyl-8-acetoxy-quinoline (8.04 g, 0.04 mol) was added in the 1,4-dioxane (60 ml) control for 3 h. The reaction mixture was heated up to 75–80°C and reacted for 4 h, then filtered and washed with dilute hydrochloric acid solution, The product was obtained by recrystallization from absolute ethanol and dried in a vacuum, with an 85% yield. ^1H NMR (400 MHz, $CDCl_3$) δ 10.22 (s, 1H, CHO), 8.32 (d, J = 8.4 Hz, 1H, ArH), 8.15 (s, 1H, OH), 8.06 (d, J = 8.5 Hz, 1H, ArH), 7.62 (t, J = 8.0 Hz, 1H, ArH), 7.43 (d, J = 7.3 Hz, 1H, ArH), 7.28 (d, J = 6.6 Hz, 1H, ArH). MS (ESI) m/z (%): 174 (M + 1, 12), 173 (M, 100), 145 (30), 117 (30), 89 (16), 63 (9).´.

2.1.3 | Synthesis of phenoxy acetic acid derivatives ($1'^{a-f}$)

As the synthesis methods for phenoxy acetic acid derivatives ($1'^{a-f}$) were very similar, only synthesis of phenoxy acetic acid ($1'^{a}$) is described. Chloroacetic acid (0.07 mol, 6.62 g) and an appropriate amount of deionized water were added into a 100 ml of a small beaker to fully dissolve chloroacetic acid, Then NaOH solution was added to obtain sodium chloroacetate solution, NaOH (0.06 mol, 2.4 g), an appropriate amount of deionized water, phenol (0.06 mol, 5.64 g) and ethanol were added into 150 ml three-necked flask, stirring was continued for reaction for 20 min. The reaction mixture was heated to 105°C and refluxed for 5 h after sodium chloroacetic acid was gradually added dropwise. The resulting mixture was acidified by using dilute HCl until the pH reached 1–2, the pure white solid compound phenoxy acetic acid ($1'^{a}$) was obtained through filtration, washed with dilute hydrochloric acid and dried, with a 78% yield. ^{1}H NMR ($CDCl_3$) δ/ppm: 7.32 (dd, J = 8.5, 7.6 Hz, 2H, ArH), 7.04 (t, J = 7.4 Hz, 1H, ArH), 7.01 (d, J = 8.6 Hz, 2H, ArH), 4.69 (s, 2H, CH_2); MS (ESI) m/z (%): 304 (2 M, 15), 303 (2 M-1, 100), 151 (M-1, 18).

p-Methyl phenoxy acetic acid ($1'^{b}$). White solid, 82% yield. ^{1}H NMR ($CDCl_3$) δ/ppm: 7.11 (d, J = 8.4 Hz, 2H, ArH), 6.83 (d, J = 8.4 Hz, 2H, ArH), 4.66 (s, 2H, CH_2), 2.30 (s, 3H, CH_3); MS (EI) m/z (%): 167 (M + 1, 9), 166 (M, 100), 121 (52), 107 (48), 91 (58), 77 (30), 65 (14).

p-Methoxy phenoxy acetic acid ($1'^{c}$). White solid, 76% yield. ^{1}H NMR ($CDCl_3$) δ/ppm: 6.90–6.84 (m, 4H, ArH), 4.66 (s, 2H, CH_2), 3.79 (s, 3H, OCH_3); MS (EI) m/z (%): 183 (M + 1, 8), 182 (M, 68), 123 (100), 109 (20), 95 (24), 77 (9).

p-Nitro phenoxy acetic acid ($1'^{d}$). White solid, 70% yield. ^{1}H NMR ($CDCl_3$) δ/ppm: 8.26 (d, J = 9.2 Hz, 2H, ArH), 6.98 (d, J = 9.2 Hz, 2H, ArH), 4.78 (s, 2H, CH_2); MS (EI) m/z (%): 198 (M + 1, 9), 197 (M, 100), 181 (10), 167 (12), 152 (86), 139 (9), 122 (19), 109 (40), 92 (30), 76 (20).

p-Chloro phenoxy acetic acid ($1'^{e}$). White solid, 88% yield. ^{1}H NMR ($CDCl_3$) δ/ppm: 7.29 (d, J = 8.4 Hz, 2H, ArH), 6.88 (d, J = 8.4 Hz, 2H, ArH), 4.68 (s, 2H, CH_2); MS (EI) m/z (%): 188 (M + 2, 33), 186 (M, 100), 141 (80), 128 (60), 111 (60), 99 (30), 75 (32).

p-Bromo phenoxy acetic acid ($1'^{f}$). White solid, 85% yield. ^{1}H NMR ($CDCl_3$) δ/ppm: 7.41 (d, J = 9.0 Hz, 2H, ArH), 6.83 (d, J = 9.0 Hz, 2H, ArH), 4.67 (s, 2H, CH_2); MS (EI) m/z (%): 232 (M + 1, 96), 230 (M-1, 100), 187 (45), 185 (50), 174 (32), 172 (32), 157 (38), 155 (34), 143 (20), 76 (18).

2.1.4 | Synthesis of phenoxy acetic acid ethyl ester derivatives ($2'^{a-f}$)

As the synthesis methods for phenoxy acetic acid ethyl ester derivative ($2'^{a-f}$) were very similar, only synthesis of phenoxyacetic acid ethyl ester ($2'^{a}$) is described. Phenoxy acetic acid (0.02 mol, 3.04 g) was dissolved in 40 ml of absolute ethanol added into a 100 ml flask and then stirred in ice water, next 1.0 ml of acetyl chloride was added dropwise, the reaction mixture was heated to 80°C and refluxed for 24 h. The phenoxy acetic acid ethyl ester compounds were obtained by removing the solvent under reduced pressure, ethanol recrystallization, and drying, with a 75% yield. ^{1}H NMR ($CDCl_3$) δ/ppm: 6.91–7.28 (m, 5H, ArH), 4.53 (s, 2H, OCH_2), 4.27 (q, J = 7.2 Hz, 2H, CH_2), 1.27 (t, J = 7.0 Hz, 3H, CH_3); MS (EI) m/z (%): 180 (M, 60), 165 (15), 151 (10), 136 (8), 108 (100), 94 (15), 77 (95).

p-Methyl phenoxy acetic acid ethyl ester ($2'^{b}$). 80% yield. ^{1}H NMR ($CDCl_3$) δ/ppm: 6.80–7.25 (m, 4H, ArH), 4.39 (s, 2H, OCH_2), 4.20 (q, J = 6.0 Hz, 2H, CH_2), 2.10 (s, 3H, CH_3); MS (EI) m/z (%): 194 (M, 50), 164 (30), 120 (100), 106 (60), 90 (80), 76 (40).

p-Methoxy phenoxy acetic acid ethyl ester ($2'^{c}$). 75% yield. ^{1}H NMR ($CDCl_3$) δ/ppm: 6.90–7.41 (m, 4H, ArH), 4.43 (s, 2H, OCH_2), 4.22 (q, J = 6.0 Hz, 2H, CH_2), 3.71 (s, 3H, OCH_3), 1.20 (t, J = 7.2 Hz, 3H, CH_3); MS (EI) m/z (%): 210 (M, 60), 180 (40), 136 (100), 122 (50), 106 (70), 75 (40).

p-Chloro phenoxy acetic acid ethyl ester ($2'^{d}$). 80% yield. ^{1}H NMR ($CDCl_3$) δ/ppm: 6.82–7.35 (m, 4H, ArH), 4.50 (s, 2H, OCH_2), 4.24 (q, J = 6.2 Hz, 2H, CH_2), 1.24 (t, J = 7.0 Hz, 3H, CH_3); MS (EI) m/z (%): 214 (M, 80), 143 (33), 141 (100), 128 (20), 112 (70), 76 (30).

p-Bromo phenoxy acetic acid ethyl ester ($2'^{e}$). 85% yield. ^{1}H NMR ($CDCl_3$) δ/ppm: 7.00–7.45 (m, 4H, ArH), 4.58 (s, 2H, OCH_2), 4.30 (q, J = 6.2 Hz, 2H, CH_2), 1.34 (t, J = 7.0 Hz, 3H, CH_3); MS (EI) m/z (%): 260 (M + 1, 20), 230 (40), 188 (100), 186 (98), 174 (30), 157 (70), 77 (40).

p-Nitro phenoxy acetic acid ethyl ester ($2'^{f}$). 75% yield. ^{1}H NMR ($CDCl_3$) δ/ppm: 6.90–7.35 (m, 4H, ArH), 4.54 (s, 2H, OCH_2), 4.38 (q, J = 6.0 Hz, 2H, CH_2), 1.24 (t, J = 7.2 Hz, 3H, CH_3); MS (EI) m/z (%): 226 (M + 1, 30), 198 (50), 154 (100), 140 (40), 124 (60), 76 (30).

2.1.5 | Synthesis of phenoxy acetyl hydrazine derivatives ($3'^{a-f}$)

As the synthesis methods for phenoxy acetyl hydrazine derivatives ($3'^{a-f}$) were very similar, only synthesis of phenoxy acetyl hydrazine ($3'^{a}$) is described. The above-mentioned phenoxy acetic acid ethyl ester (0.01 mol, 1.80 g) and 30 ml ethanol were added into a 100 ml flask and 80% hydrazine hydrate (10 ml) was added dropwise when mixture temperature reached 85°C and refluxed for 4–5 h, the reaction mixture was cooled, filtered, washed, and dried. The target product phenoxy acetyl hydrazide ($3'^{a}$) was obtained by recrystallization from ethanol. White crystals, 88% yield. ^{1}H NMR ($CDCl_3$) δ/ppm: 7.80 (s, 1H, NH), 7.36 (t, J = 7.9 Hz, 2H, ArH), 7.06 (t, J = 7.4 Hz, 1H, ArH), 6.94 (d, J = 8.5 Hz, 2H, ArH), 4.61 (s, 2H, CH_2), 3.92 (s, 2H, NH_2); MS (EI) m/z (%): 167 (M + 1, 6), 166 (M, 36), 135 (4), 134 (10), 108 (6), 107 (25), 94 (100), 77 (66), 65 (8).

p-Methyl phenoxy acetyl hydrazide ($3'^{b}$). White crystals, 85% yield. ^{1}H NMR ($CDCl_3$) δ/ppm: 7.75 (s, 1H, NH), 7.11 (d, J = 8.4 Hz, 2H, ArH), 6.80 (d, J = 8.4 Hz, 2H, ArH), 4.54 (s, 2H, CH_2), 3.91 (s, 2H, NH_2), 2.32 (s, 3H, CH_3); MS (EI) m/z (%): 181 (M + 1, 4), 180 (M, 20), 122 (4), 121 (14), 108 (100), 107 (18), 91 (56), 77 (9), 65 (9).

p-Methoxy phenoxy acetyl hydrazide ($3'^{c}$). White crystals, 86% yield. ^{1}H NMR ($CDCl_3$) δ/ppm: 7.72 (s, 1H, NH), 6.90–6.81 (m, 4H, ArH), 4.54 (s, 2H, CH_2), 3.92 (s, 2H, NH_2), 3.76 (s, 3H, OCH_3); MS (EI) m/z (%): 197 (M + 1, 6), 196 (M, 28), 138 (10), 137 (11), 124 (100), 109 (30), 107 (18), 92 (9), 77 (18), 64 (8).

p-Chloro phenoxy acetyl hydrazide ($3'^{d}$). White crystals, 90% yield. ^{1}H NMR ($CDCl_3$) δ/ppm: 7.72 (s, 1H, NH), 7.30 (d, J = 9.0 Hz, 2H, ArH), 6.87 (d, J = 9.0 Hz, 2H, ArH), 4.56 (s, 2H, CH_2), 3.95 (s, 2H, NH_2); MS (EI) m/z (%): 202 (M + 2, 10), 200 (M, 18), 143 (8), 141 (16), 130 (35), 128 (100), 111 (32), 99 (8), 77 (10), 65 (6).

p-Bromo phenoxy acetyl hydrazide (3′[e]). White crystals, 87% yield. ^{1}H NMR ($CDCl_3$) δ/ppm: 7.69 (s, 1H, NH), 7.42 (d, J = 9.0 Hz, 2H, ArH), 6.80 (d, J = 9.0 Hz, 2H, ArH), 4.56 (s, 2H, CH_2), 3.94 (s, 2H, NH_2); MS (EI) m/z (%): 246 (M + 1, 18), 244 (M-1, 18), 187 (14), 185 (20), 174 (94), 172 (100), 157 (50), 155 (48), 145 (10), 143 (6), 106 (9), 93 (10), 77 (20), 65 (22).

p-Nitro phenoxy acetyl hydrazide (3′[f]). Yellowish crystals, 82% yield. ^{1}H NMR ($CDCl_3$) δ/ppm: 8.25 (d, J = 8.0 Hz, 2H, ArH), 7.63 (s, 1H, NH), 7.00 (d, J = 8.0 Hz, 2H, ArH), 4.66 (s, 2H, CH_2), 3.96 (s, 2H, NH_2); MS (EI) m/z (%): 212 (M + 1, 8), 211 (M, 24), 153 (8), 152 (26), 123 (14), 122 (22), 106 (10), 92 (14), 76 (16), 73 (100), 65 (8).

2.2 | Synthesis of the target compounds

As the synthesis methods for the 2-formyl-8-hydroxyquinoline phenoxy acetyl hydrazine derivatives (Y^{1-6}) were similar, only synthesis of the 2-formyl-8-hydroxyquinoline phenoxy acetyl hydrazide (Y^1) is described. 2-Formyl-8-hydroxyquinoline (5 mmol, 0.865 g) and 30 ml of absolute ethanol were added into a 100 ml three-necked flask and heated to 80°C until fully dissolved. Phenoxy acetyl hydrazide (4 mmol, 0.664 g) was dissolved in 20 ml of absolute ethanol, and then slowly added dropwise into a 100 ml three-necked flask, and an appropriate amount of acetic acid was added as a catalyst. The reaction mixture was stirred at reflux for 5 h, filtered and washed several times. The 2-formyl-8-hydroxyquinoline phenoxy acetyl hydrazide (Y^1) was obtained by recrystallization from absolute ethanol and dried in a vacuum.

2-Formyl-8-hydroxyquinoline phenoxy acetyl hydrazide (Y^1). Red solid, 72% yield. m.p. 158–160°C; ^{1}H NMR (400 MHz, DMSO) δ 12.05 (s, 1H, N–NH), 9.91 (s, 1H, CH=N), 8.34 (d, J = 8.6 Hz, 1H, ArH), 8.25 (s, 1H, OH), 8.13 (d, J = 8.7 Hz, 1H, ArH), 7.53–7.38 (m, 2H, ArH), 7.32 (dd, J = 14.5, 6.7 Hz, 2H, ArH), 7.13 (d, J = 6.3 Hz, 1H, ArH), 6.99 (dt, J = 19.6, 9.9 Hz, 3H, ArH), 5.26 (s, 2H, CH_2); MS (EI) m/z (%): 322 (M + 1, 12), 321 (M, 52), 214 (29), 187 (14), 186 (100), 158 (84), 131 (17), 130 (46), 103 (14), 77 (34).

2-Formyl-8-hydroxyquinoline *p*-methyl phenoxy acetyl hydrazide (Y^2). Red solid, 80% yield. m.p. 161–162°C; ^{1}H NMR (400 MHz, DMSO) δ 11.99 (s, 1H, N–NH), 9.90 (s, 1H, CH=N), 8.33 (d, J = 8.6 Hz, 1H, ArH), 8.23 (s, 1H, OH), 8.11 (d, J = 8.7 Hz, 1H, ArH), 7.52–7.26 (m, 2H, ArH), 7.12 (dd, J = 15.1, 6.9 Hz, 3H, ArH), 6.89 (dd, J = 20.7, 8.4 Hz, 2H, ArH), 5.20 (s, 2H, CH_2), 2.21 (s, 3H, CH_3); MS (EI) m/z (%): 337 (M + 2, 2), 336 (M + 1, 12), 335 (M, 47), 214 (30), 187 (14), 186 (100), 158 (85), 130 (43), 91 (22).

2-Formyl-8-hydroxyquinoline *p*-methoxy phenoxy acetyl hydrazide (Y^3). Red solid, 82% yield. m.p. 168–170°C; ^{1}H NMR (400 MHz, DMSO) δ 12.01 (s, 1H, N–NH), 9.90 (s, 1H, CH=N), 8.33 (d, J = 8.6 Hz, 1H, ArH), 8.23 (s, 1H, OH), 8.11 (d, J = 8.7 Hz, 1H, ArH), 7.43 (dd, J = 16.7, 7.7 Hz, 2H, ArH), 7.13 (t, J = 6.4 Hz, 1H, ArH), 7.00–6.82 (m, 4H, ArH), 5.18 (s, 2H, CH_2), 3.70 (s, 3H, CH_3); MS (EI) m/z (%): 352 (M + 1, 15), 351 (M, 64), 187 (12), 186 (100), 158 (93), 145 (14), 130 (55), 124 (17), 109 (15), 103 (14).

2-Formyl-8-hydroxyquinoline *p*-chloro phenoxy acetyl hydrazide (Y^4). Red solid, 85% yield. m.p. 200–202°C; ^{1}H NMR (400 MHz, DMSO) δ 12.00 (s, 1H, N-NH), 9.85 (s, 1H, CH=N), 8.33 (d, J = 8.7 Hz, 1H), 8.24 (s, 1H, OH), 8.12 (d, J = 8.6 Hz, 1H, ArH), 7.56–7.25 (m, 4H, ArH), 7.12 (d, J = 7.0 Hz, 1H, ArH), 7.03 (dd, J = 16.1, 8.8 Hz, 2H, ArH), 5.27 (s, 2H, CH_2); MS (EI) m/z (%): 358 (M + 3, 7), 357 (M + 2, 28), 355 (M, 80), 214 (38), 187 (13), 186 (100), 158 (65), 130 (27), 111 (10).

2-Formyl-8-hydroxyquinoline *p*-bromo phenoxy acetyl hydrazide (Y^5). Red solid, 88% yield. m.p. 214–216°C; ^{1}H NMR (400 MHz, DMSO) δ 12.05 (s, 1H, N-NH), 9.90 (s, 1H, CH=N), 8.49 (d, J = 11.3 Hz, 1H, ArH, 8.34 (d, J = 8.7 Hz, 1H, ArH), 8.23 (s, 1H, OH), 8.12 (d, J = 8.9 Hz, 1H, ArH), 7.53–7.37 (m, 4H, ArH), 7.13 (t, J = 6.3 Hz, 1H, ArH), 6.97 (t, J = 7.6 Hz, 2H, ArH), 5.28 (s, 2H, CH_2); MS (EI) m/z (%): 403 (M + 3, 12), 401 (M + 1, 13), 214 (24), 187 (13), 186 (100), 158 (79), 130 (45), 103 (13), 77 (11).

2-Formyl-8-hydroxyquinoline *p*-nitro phenoxy acetyl hydrazide (Y^6). Red solid, 76% yield. m.p. 220–222°C; ^{1}H NMR (400 MHz, DMSO) δ 12.11 (s, 1H, N–NH), 9.93 (s, 1H, CH=N), 8.49 (t, J = 8.4 Hz, 1H, ArH), 8.35 (d, J = 8.7 Hz, 1H, ArH), 8.26–8.20 (m, 2H, ArH, 1H, OH), 8.15 (d, J = 8.1 Hz, 1H, ArH), 7.51–7.38 (m, 2H, ArH), 7.21 (d, J = 9.2 Hz, 2H, ArH), 7.13 (d, J = 7.3 Hz, 1H, ArH), 5.48 (s, 2H, CH_2); MS (EI) m/z (%): 367 (M + 1, 3), 366 (M, 18), 308 (10), 214 (17), 186 (92), 158 (100), 145 (16), 131 (30), 130 (65), 103 (22), 102 (17), 77 (14).

2.3 | Synthesis of the target Eu(III) complexes

As the synthesis and purification of the target europium complexes were similar, only the synthesis of the europium complexes of compound Y^1 is described. A mixture of compound Y^1 (0.50 mmol) and absolute ethanol (40 ml) was added into a 100 ml three-neck flask and refluxed at 60°C for some time, and then 5 ml $Eu(NO_3)_3$ (0.1 mol L^{-1}) ethanol solution was added. When the precipitate was formed, the mixture was continuously refluxed for 4.5 h, with hot suction filtration, the product was washed several times with absolute ethanol, filtered and dried in a vacuum for 8 h.

2.3.1 | Solubility, elemental analysis and molar conductivity of the Eu(III) complexes

The target ligands Y^{1-6} were easily dissolved in strong polar solvents such as dimethyl sulfoxide (DMSO) and dimethyl formamide (DMF). They were soluble in hot chloroform and hot ethanol, and insoluble in benzene and cyclohexane. While the Eu(III) complexes were soluble in DMF and DMSO, slightly soluble in hot chloroform and hot ethanol and other solvents, they were insoluble in benzene, ether and other less polar solvents.

The elemental analysis and molar conductivity data of Eu(III) complexes at room temperature are given in Table 1.

It can be seen from Table 1 that the experimental data of the target europium complexes were consistent with the theoretical values, indicating that the composition of the target complexes were $EuY^{1-6}(NO_3)_3.2H_2O$, and three nitrate molecules were also coordinated to the europium ion. The molar conductivity of $EuY^{1-6}(NO_3)_3.2H_2O$ in DMF (10^{-3} mol.L^{-1}) solution at room temperature solution was less than 65 S.cm^2.mol^{-1}, which indicated that the target europium complexes were non-electrolytes.[15]

2.3.2 | IR spectral analysis

The IR spectra data of the ligands Y^{1-6} and their corresponding Eu(III) complexes are presented in Table 2. As the IR spectra of the

TABLE 1 Elemental analysis and molar conductivity data of Eu(III) complexes

Complexes	Found (calculated) (%)				Λm (S.cm^2.mol^{-1})
	C	H	N	Eu	H
$EuY^1(NO_3)_3.2H_2O$	31.38 (31.08)	2.14 (2.73)	12.75 (12.09)	21.87 (21.87)	20
$EuY^2(NO_3)_3.2H_2O$	32.01 (32.16)	2.31 (2.96)	11.16 (11.85)	21.27 (21.44)	21
$EuY^3(NO_3)_3.2H_2O$	31.76 (31.45)	2.69 (2.90)	11.58 (11.59)	21.86 (21.02)	17
$EuY^4(NO_3)_3.2H_2O$	30.41 (29.63)	2.65 (2.47)	11.85 (11.52)	20.43 (20.85)	18
$EuY^5(NO_3)_3.2H_2O$	28.19 (27.94)	2.51 (2.32)	10.09 (10.87)	19.23 (19.66)	15
$EuY^6(NO_3)_3.2H_2O$	30.14 (29.19)	2.68 (2.43)	13.32 (13.24)	20.74 (20.54)	19

complexes are similar, only the spectra of $EuY^5(NO_3)_3.2H_2O$ and the corresponding ligand Y^5 are illustrated, as shown in Figure 1.

As shown in the Table.2 and Figure 1, compared with the ligand IR spectra curve a, the IR absorption curve b of the target complex $EuY^5(NO_3)_3.2H_2O$ was changed. The characteristic absorption peaks of the functional groups were changed and shifted. The vibrational absorption peaks of the C=O functional groups were shifted, $\nu_{c=o}$ from 1692 cm^{-1} in Y^5 to 1687 cm^{-1} in $EuY^5(NO_3)_3.2H_2O$, which confirmed that the oxygen atom of the amide group was coordinated to the Eu(III) ion. The absorption peak of Ar–N on the quinoline ring was shifted from 1545 cm^{-1} to 1508 cm^{-1}, which indicated that the N atom of the Ar–N was coordinated with the europium ion. The absorption peak of Ar–O–C on the hydroxyl-quinoline ring was also red shifted to 1108 cm^{-1}, which may be due to the formation of the coordination compound Y^1 and Eu^{3+} that led to a decrease in the stretching vibration frequency and red shift. This result indicated that the O atom of the Ar–O–C functional group of the hydroxyl-quinoline ring was involved in the coordination of the europium ions. The CH=N bond between the two benzene rings was clearly red shifted to 1558 cm^{-1}. This result indicated that the N atom of the CH=N functional group participates in the coordination. In addition, the characteristic absorption peak of nitrate was observed in the IR spectrum of $EuY^5(NO_3)_3.2H_2O$, and the asymmetric stretching vibration absorption peak (ν_{as}) of NO_3^{-1} appeared near 1487 cm^{-1}, its symmetric stretching vibration absorption peak (ν_s) of NO_3^{-1} appeared near 1386 cm^{-1}, $|\nu_{as} - \nu_s|$ of the target complex $EuY^5(NO_3)_3.2H_2O$ was 101 cm^{-1}, which is less than 200 cm^{-1}, so it can be considered that

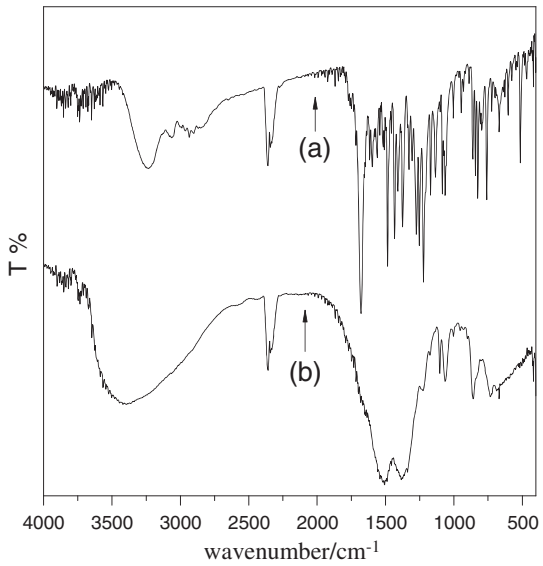

FIGURE 1 IR spectra of $EuY^5(NO_3)_3.2H_2O$ (b) and Y^5 (a)

the complex formed between the NO_3^{-1} and the europium ion adopts a bidentate coordination form.[16] There was no characteristic absorption peak of free NO_3^{-1} from the figure, which indicated that three NO_3^{-1} in the target complexes were involved in the coordination. The result of this analysis agrees with the measured result in molar conductivity.

TABLE 2 IR data (cm^{-1}) of ligands Y^{1-6} and their Eu(III) complexes

Compounds	ν(O–H)	ν(Ar–N)	Hydrazide		ν(Ar–O–C)	ν(NO^{3-})			
			ν(C=O)	ν(C=N)		ν_1	ν_4	ν_2	ν_3
Y^1	3419	1539	1689	1602	1144				
$EuY^1(NO_3)_3.2H_2O$	3384	1505	1679	1560	1101	1484	1388	1062	851
Y^2	3416	1537	1687	1618	1131				
$EuY^2(NO_3)_3.2H_2O$	3392	1505	1680	1555	1104	1487	1384	1064	850
Y^3	3402	1538	1676	1615	1130				
$EuY^3(NO_3)_3.2H_2O$	3376	1506	1672	1562	1107	1491	1386	1066	852
Y^4	3408	1538	1693	1591	1168				
$EuY^4(NO_3)_3.2H_2O$	3388	1509	1686	1560	1105	1485	1385	1062	852
Y^5	3410	1545	1692	1603	1158				
$EuY^5(NO_3)_3.2H_2O$	3364	1508	1687	1558	1108	1487	1386	1064	850
Y^6	3409	1559	1701	1594	1173				
$EuY^6(NO_3)_3.2H_2O$	3382	1503	1697	1159	1110	1493	1384	1068	845

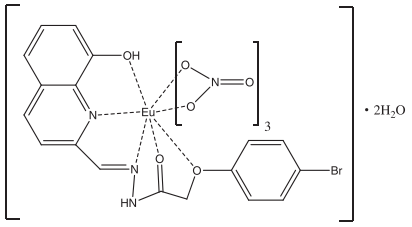

FIGURE 2 Molecular structure of the complex $EuY^5(NO_3)_3.2H_2O$

Based on elemental analysis, molar conductivity and IR spectroscopy, the possible molecular structure of the complex $EuY^5(NO_3)_3.2H_2O$ can be deduced and is shown in Figure 2.

3 | RESULTS AND DISCUSSION

3.1 | UV spectra analysis

The UV spectral data and the molar absorption coefficient (ε) of the ligands Y^{1-6} and their corresponding target complexes were recorded in DMSO solution (10^{-4} mol. L^{-1}), as listed in Table 3. As the UV spectra of the complexes are similar, only the UV spectra of $EuY^2(NO_3)_3.2H_2O$ and the corresponding ligand Y^2 are illustrated, as shown in Figure 3.

As shown in Table 3, the λ_{max} (maximum absorption wavelength) of Eu(III) complexes were higher than that of the corresponding ligands. The K absorption peak of the π–π* transition of the target ligand Y^{1-6} was in the range 284–299 nm, and the range from n–π* transition was 326–332 nm. The UV absorption peak of π–π* transition and n–π* transition of the target europium complex $EuY^{1-6}(NO_3)_3.2H_2O$ were red shifted for different degrees. This result indicated that the europium ion was successfully coordinated with the target ligand. As shown in Figure 3, the absorption intensity of the complex $EuY^2(NO_3)_3.2H_2O$ was higher than that of ligand Y^2. The spectra showed that the π–π* absorption peak was shifted from 285 nm in Y^2 to 289 nm in $EuY^2(NO_3)_3.2H_2O$, the n–π* absorption peak was shifted from 331 nm in Y^2 to 340 nm in $EuY^2(NO_3)_3.2H_2O$. This result is due to the coordination of ligand Y^2 with Eu^{3+} ions, which increased the electron cloud density of the ligand, enhanced its conjugation and reduced the energy required for the transition. These phenomena resulted from the extended conjugated system by coordination of the ligand Y^2 with the Eu(III) ion.[17]

TABLE 3 UV spectral data of the ligand and their Eu(III) complexes

Compounds	λ_1 (nm)	ε_1 (1.0×10^4 $L.mol^{-1}.cm^{-1}$)	λ_2 (nm)	ε_2 (1.0×10^4 $L.mol^{-1}.cm^{-1}$)
Y^1	286	1.03	330	0.71
$EuY^1(NO_3)_3.2H_2O$	290	1.14	340	0.79
Y^2	285	1.03	331	0.73
$EuY^2(NO_3)_3.2H_2O$	289	1.10	340	0.76
Y^3	295	1.01	332	0.61
$EuY^3(NO_3)_3.2H_2O$	299	1.15	340	0.67
Y^4	284	1.01	326	0.58
$EuY^4(NO_3)_3.2H_2O$	288	1.13	339	0.66
Y^5	285	1.06	326	0.70
$EuY^5(NO_3)_3.2H_2O$	290	1.18	340	0.73
Y^6	290	1.09	331	0.80
$EuY^6(NO_3)_3.2H_2O$	293	1.25	342	0.82

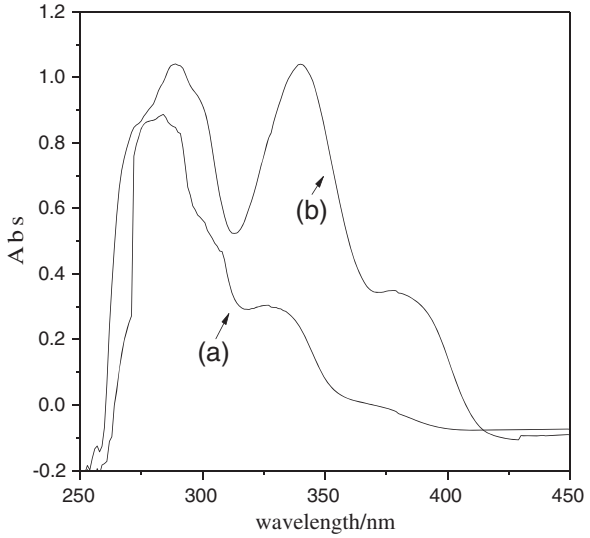

FIGURE 3 UV spectra of $EuY^2(NO_3)_3.2H_2O$ (b) and Y^2 (a)

3.2 | Thermal analysis

The endothermic peak, exothermic peak and residual weight of the Eu(III) complexes $EuY^{1-6}(NO_3)_3.2H_2O$ in thermogravimetric–differential thermal analysis (TG–DTA) are shown in Table 4. As the thermal behaviours of all the complexes were very similar, only the TG–DTA curves of $EuY^4(NO_3)_3.2H_2O$ are depicted, as shown in Figure 4.

As shown in Table 4 and Figure 4, the TG–DTA curve of europium complex $EuY^4(NO_3)_3.2H_2O$ presented a slight mass loss between 50 and 120°C, and a small endothermic peak appeared on the DTA curve at the corresponding temperature, which may be due to the small amount of absorbed water in the test sample. There was a mass loss at 120–220°C in TG curve, and a small endothermic peak appears at 189°C on the DTA curve, which was attributed to the two molecular water crystals in the target complex, the measured mass loss rate was 5.00%, these data and the theoretical value 4.94% were basically consistent. We found that the TG curve of $EuY^4(NO_3)_3.2H_2O$ at 250–450°C showed a very obvious mass loss, it was 49.10% which is basically consistent with the theoretical value of 48.70%, two obvious exothermic peaks appeared at 270°C and 438°C. These data showed that the ligand Y^4 in $EuY^4(NO_3)_3.2H_2O$ gradually decomposed to completion at this temperature range. The TG curve of the europium complex showed a mass loss of 25.85%

TABLE 4 TG–DTA data of the Eu(III) complexes

Complexes	Endothermic peak (°C)	Exothermic peak (°C)	Metal residue (calculated) (%)
$EuY^1(NO_3)_3.2H_2O$	65, 160	338, 488, 616	22.31 (21.87)
$EuY^2(NO_3)_3.2H_2O$	74, 180	439, 553	22.45 (21.44)
$EuY^3(NO_3)_3.2H_2O$	80, 190	326, 472	22.12 (20.97)
$EuY^4(NO_3)_3.2H_2O$	63, 189	270, 438, 516	21.20 (20.85)
$EuY^5(NO_3)_3.2H_2O$	95, 206	348, 536	20.64 (19.66)
$EuY^6(NO_3)_3.2H_2O$	91, 190	346, 506	22.02 (20.54)

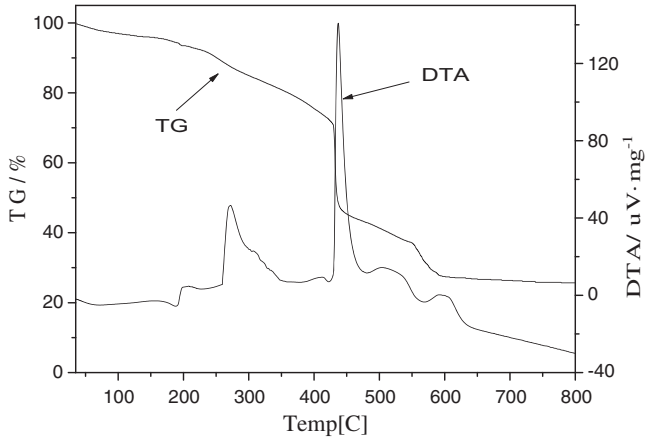

FIGURE 4 TG–DTA curves of $EuY^4(NO_3)_3.2H_2O$

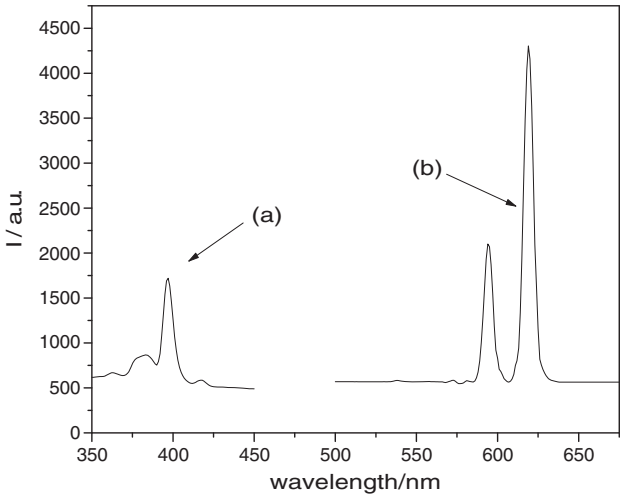

FIGURE 5 Excitation spectra (a) and emission spectra (b) of $EuY^3(NO_3)_3.2H_2O$

at 450–650°C, an exothermic peak appeared at 516°C on the DTA curve, this was due to loss of three nitrates ions, and the experimental data were close to the theoretical value (25.51%). The target complex $EuY^4(NO_3)_3.2H_2O$ completely decomposed when the temperature exceeded 650°C, the residue was Eu_2O_3.[18] The mass percentage was 21.20%, which was consistent with the theoretical value 20.85%. The thermal analysis results showed the target complexes exhibited high thermal stabilities.

3.3 | Luminescence properties analysis

The corresponding luminescence spectral data are summarized in Table 5. As the luminescence spectra of the complexes were very similar, only the luminescence spectra of $EuY^3(NO_3)_3.2H_2O$ are illustrated. The excitation and emission spectra of europium complexes $EuY^3(NO_3)_3.2H_2O$ are shown in Figure 5.

As shown in Table 5 and Figure 5, all Eu(III) complexes presented the characteristic red luminescence of Eu^{3+} ions. This result indicated that the ligands Y^{1-6} can coordinate well with Eu^{3+} ions. The emission peaks at 595 nm and 619 nm were attributed to the $^5D_0 \rightarrow {}^7F_1$ (magnetic dipole transition) and $^5D_0 \rightarrow {}^7F_2$ (electric dipole transition) of Eu^{3+} ions, respectively.[19] It is known that the $^5D_0 \rightarrow {}^7F_1$ (magnetic dipole transition) in the europium complex is almost independent of the ligand environment, whereas the $^5D_0 \rightarrow {}^7F_2$ (electric dipole transition) is sensitive to the coordination environment. The ligand in the Eu(III) complex absorbs energy and undergoes a π–π^* transition, the electron transitions from the ground state of the singlet state to the lowest excited singlet state, then intersystem crossing occurs to the excited state of the triplet state in a non-radiative manner. The excited state of triplet state transfers energy to the vibrational energy level of the europium ion by the vibrational coupling of the chemical bond. Energy in the excited state of europium ion transitions from a high energy state to a low energy state in a radiative manner, emitting fluorescence. At the same time, its emission peak at 619 nm is narrow and sharp, and no other peaks appear, which indicated that the target complexes had high colour purity.

The intramolecular energy transfer efficiency of organic ligands and central europium ions is the most important factor affecting the luminescence properties of the complexes. The difference between the lowest triplet energy level of the ligand and the resonance emission level of the central ion decreases, and both the energy transfer rate and the inverse energy transfer rate increased. So there was a best match between the two values, if the difference is too large or too small it will reduce the luminescence properties of the Eu(III) complexes. Therefore, the triplet energy level of the ligand must be higher than the excited state energy level of the europium ions to produce energy resonance transmission, otherwise no fluorescence will be generated. However, if the triplet energy level of the ligand is much higher than the excited state energy level of the europium ions, the effective resonance transfer of the energy cannot occur because the spectral overlap is small. If the difference between the triplet level of the ligand and the excited state of the rare earth ion is too small, the thermal deactivation rate of the triplet state of the ligand is larger than that of the energy transfer to the rare earth ions, and no effective energy transfer occurs. As shown in Table 5, the luminescence intensity of the Eu(III) complexes series was affected by the type of ligand substituents. The introduction of electron-donating groups (–OCH_3, –CH_3, –H) can enhance the luminescence intensity of the target complexes, and the introduction of electron-withdrawing groups (–Cl, –Br, –NO_2) impaired the luminescence intensity of the target complexes. From the above analysis, it can be seen that $EuY^3(NO_3)_3.2H_2O$ had the highest luminescence intensity, indicating that the resonance emission level of Y^3 and Eu^{3+} possessed the best match and the energy transfer efficiency was the highest.

TABLE 5 Luminescence spectral data and peak attributed of Eu(III) complexes

Complexes	λ_{ex} (nm)	I (a.u.)	$^5D_0 \rightarrow {}^7F_1$		$^5D_0 \rightarrow {}^7F_2$	
			λ_{em} (nm)	I (a.u.)	λ_{em} (nm)	I (a.u.)
$EuY^1(NO_3)_3.2H_2O$	396	1367	594	1159	618	3935
$EuY^2(NO_3)_3.2H_2O$	396	1376	595	1871	620	4148
$EuY^3(NO_3)_3.2H_2O$	397	1716	595	2098	619	4320
$EuY^4(NO_3)_3.2H_2O$	396	2476	594	956	619	2858
$EuY^5(NO_3)_3.2H_2O$	395	1359	592	844	617	2739
$EuY^6(NO_3)_3.2H_2O$	392	1084	594	774	618	2187

TABLE 6 Fluorescence quantum yields data of the Eu(III) complexes

Complexes	Absorption wavelength (λ/nm)	Fluorescence intensity (I/a.u.)	Fluorescence quantum yield (Φ_{fx})
$EuY^1(NO_3)_3.2H_2O$	327	2250	0.507
$EuY^2(NO_3)_3.2H_2O$	324	2470	0.547
$EuY^3(NO_3)_3.2H_2O$	316	2740	0.628
$EuY^4(NO_3)_3.2H_2O$	319	1890	0.473
$EuY^5(NO_3)_3.2H_2O$	314	1680	0.452
$EuY^6(NO_3)_3.2H_2O$	321	1120	0.396

3.4 | Fluorescence quantum yields analysis

The fluorescence quantum yields data of all europium complexes are summarized in Table 6.

As shown in the Table 6, the fluorescence quantum yields of the Eu(III) complexes was in order $EuY^3(NO_3)_3.2H_2O$ > $EuY^2(NO_3)_3.2H_2O$ > $EuY^1(NO_3)_3.2H_2O$ > $EuY^4(NO_3)_3.2H_2O$ > $EuY^5(NO_3)_3.2H_2O$ > $EuY^6(NO_3)_3.2H_2O$, which was in agreement with the fluorescence properties. The more matched the resonance energy level of the Eu(III) ions and the triplet energy level of the ligand, the more effective the intramolecular energy transfer. The europium complex introduced electron-donating groups (–CH3, –OCH3, –H) to increase the electron density and the conjugation of the π bond system in the europium complex, and increased the fluorescence quantum yields. The introduction of electron-withdrawing groups (–Cl, –Br, $–NO_2$) weakened the conjugation effect and increased the difference in energy level between the triplet state of the ligand and the resonance energy level of the Eu (III) ion. So energy transfer efficiency and emission quantum yield decreased. $EuY^3(NO_3)_3.2H_2O$ had the highest fluorescence quantum yield, which showed that the resonance energy level of Eu(III) ion is most compatible with the triplet energy level of the ligand Y^3, and the energy transfer efficiency is the highest.

4 | CONCLUSION

With 2-methyl-8-hydroxyquinoline and para-substituted phenol as the main starting materials, first, 2-methyl-8-hydroxyquinoline and acetic anhydride were refluxed to obtain the intermediate. Then, 1,4-dioxane was used as the solvent and SeO_2 as the catalyst and were oxidized to obtain 2-formyl-8-hydroxyquinoline. Finally, a series of 8-hydroxyquinoline derivatives and their complexes with Eu(III) was prepared successfully, and characterized by elemental analysis, molar conductance, thermogravimetric analysis, and UV and IR light analyses. The luminescence analysis results indicated that all complexes showed the characteristic luminescence of the Eu(III) ion. The thermal analysis results showed that the target complexes exhibited high thermal stabilities. The luminescence intensity of the complexes was enhanced by the introduction of electron-donating groups. $EuY^3(NO_3)_3.2H_2O$ had the highest luminescence intensity with the highest fluorescence quantum yield among all target complexes and was up to 0.628. The fluorescence quantum yields of the complexes with electron-donating groups increased and the fluorescence quantum yield of the complexes with electron-withdrawing groups decreased. These Eu(III) complexes may possibly have significance for use as fluorescent anti-counterfeiting materials, luminous paint and fluorescent probes, and in other fields of interest.

ACKNOWLEDGEMENTS

The authors are grateful for the financial support of the National Natural Science Foundation of China (No. J1103312; No. J1210040; No. 21341010), the Natural Science Foundation of Hunan Province (No. 11JJ5005), Hunan Provincial Science&Technology Department (No. 2016SK2064), Changsha Science&Technology Bureau (No. kq1701029; No. kq1701164), the Innovative Research Team in University (No. IRT1238), and China Outstanding Engineer Training Plan for Students of Chemical Engineering & Technology in Hunan University (MOE-No. 2011-40).

ORCID

Yongqiang Wu http://orcid.org/0000-0002-5147-4201

REFERENCES

[1] M. H. Kaulage, B. Maji, S. Pasadi, S. Bhattacharya, K. Muniyappa, *Eur. J. Med. Chem.* **2017**, *139*, 1016.

[2] W. M. Wan, S. S. Li, D. M. Liu, X. H. Lv, X. L. Sun, *Macromolecules* **2017**, *50*, 6872.

[3] Y. Zhu, A. Bao, B. Na, G. Su, J. Wanga, J. Langa, *RSC Adv.* **2017**, *7*, 3586.

[4] R. Sarkar, P. Mondal, K. K. Rajak, *Dalton Trans.* **2014**, *43*, 2859.

[5] Y. Cui, Y. Yue, G. Qian, B. Chen, *Chem. Rev.* **2012**, *112*, 1126.

[6] E. Coronado, G. M. Espallargas, *Chem. Soc. Rev.* **2013**, *42*, 1525.

[7] E. D. Bloch, W. L. Queen, R. Krishna, J. M. Zadrozny, C. M. Brown, J. R. Long, *Science* **2012**, *335*, 1606.

[8] M. Yoon, R. Srirambalaji, K. Kim, *Chem. Rev.* **2012**, *112*, 1196.

[9] X. Q. Song, L. Wang, M. M. Zhao, G. Q. Cheng, X. R. Wang, Y. Q. Peng, *Inorg. Chim. Acta* **2013**, *402*, 156.

[10] D. Meng, F. Liu, Y. Li, Z. Yang, G. Li, D. Guo, *Luminescence* **2016**, *31*, 507.

[11] Y. Qu, X. Lin, A. Wang, Z. Wang, J. K. H. Chu, Y. Zhao, *JOL* **2014**, *154*, 402.

[12] K. Nakagawa, K. Amita, H. Mizuno, Y. Inoue, T. Hakushi, *Bull. Chem. Soc. Jpn.* **1987**, *60*, 2037.

[13] B. Zhang, X. Xu, Q. Li, Y. Wu, J. Qiu, X. Yu, *J. Solid State Chem.* **2014**, *217*, 136.

[14] Y. X. Ci, X. Jia, *Chin. J. Anal. Chem.* **1986**, *14*, 616.

[15] W. J. Geary, *Coord. Chem. Rev.* **1971**, *7*, 81.

[16] K. P. Zhuravlev, A. V. Vologzhanina, V. A. Kudryashova, Z. S. Klemenkova, V. I. Tsaryuk, *Polyhedron* **2013**, *56*, 109.

[17] W. Zhang, W. He, X. Guo, Y. Chen, L. Wu, D. Guo, *J. Alloys Compd.* **2015**, *620*, 383.

[18] M. R. Dousti, M. R. Sahar, M. S. Rohani, A. Samavati, Z. A. Mahraz, R. J. Amjad, A. Awang, R. Arifin, *J. Mol. Struct.* **2014**, *1065*, 39.

[19] H. Wang, X. Zhao, M. Liu, W. Shi, P. Cheng, *Chin. J. Chem.* **2012**, *30*, 2097.

How to cite this article: Wu Y, Guo T, Shu D, et al. Synthesis and luminescence properties of novel 8-hydroxyquinoline derivatives and their Eu(III) complexes. *Luminescence*. 2018; 1–8. https://doi.org/10.1002/bio.3482